Decorrelation-based Concurrent Digital Predistortion with a Single Feedback Path

Mahmoud Abdelaziz, *Student Member, IEEE,* Lauri Anttila, *Member, IEEE,* Adnan Kiayani, *Member, IEEE,* Mikko Valkama, *Senior Member, IEEE,*

***Abstract*—In this article, a novel decorrelation-based concurrent digital predistortion (DPD) solution is proposed for dual-band transmitters employing a single wideband power amplifier (PA), and utilizing only a single feedback receiver path. The proposed decorrelation-based parameter learning solution is both flexible and simple, and operates in a closed-loop manner, opposed to the widely-applied indirect learning architecture. The proposed decorrelation-based learning and DPD processing can also be effectively applied to more ordinary single carrier/band transmissions, as well as generalized to more than two transmit bands. Through a comprehensive analysis covering both the DPD parameter learning and the main path processing, it is shown that the complexity of the proposed concurrent DPD is substantially lower compared to the other state-of-the-art concurrent DPD methods. Extensive set of simulation and RF measurement results are also presented, using base-station PAs as well as a commercial LTE-Advanced mobile PA, to evaluate and validate the effectiveness of the proposed DPD solution in various real world scenarios, incorporating both single-band and dual-band transmitter cases. The simulation and RF measurement results demonstrate excellent linearization performance of the proposed concurrent DPD, even outperforming current state-of-the-art methods, despite the significantly lower complexity.**

***Index Terms*—Adaptive filters, carrier aggregation, concurrent linearization, digital predistortion, dual band power amplifiers, frequency division duplexing, nonlinear distortion, spectrally agile radio, 3GPP LTE-Advanced.**

I. Introduction

SPECTRUM aggregation improves the achievable bit-rates and the efficiency of the radio spectrum utilization, but also poses substantial challenges in the transmitter design, especially in low-cost devices such as mobile terminals and small-cell base-stations [1]. In order to enhance the power and cost efficiencies of such wideband transmitters, e.g., carrier aggregation (CA) transmitters in 3GPP LTE-Advanced, the component carriers (CCs) should be combined prior to the power amplifier (PA) [2], in particular in cases where the CCs are still relatively close in frequency. However, this leads to additional unwanted emissions due to inter-modulation between the CCs, as a result of the PA nonlinearity [3], as shown in Fig. 1.

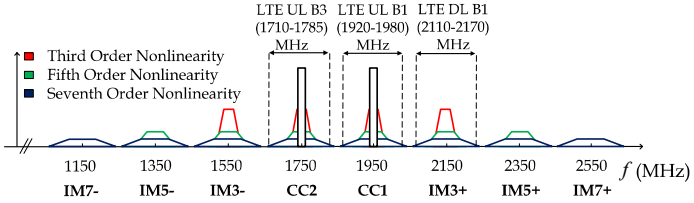

Fig. 1. Illustration of different distortion components created by a nonlinear PA when excited with a non-contiguous CA signal with two component carriers. In this LTE-A UL interband CA example, the CCs are at LTE UL bands 1 and 3. In addition to the EVM and ACLR degradation due to distortion components at and around the main CCs, the IM3+ spur lies at the own RX frequencies of Band 1, causing own RX desensitization.

Three kinds of unwanted emissions result from the nonlinear behavior. The first is emitted in-band, right on top of each CC, thus degrading the in-band error vector magnitude (EVM). The second kind of emissions are out-of-band (OOB) emissions which are emitted in the adjacent channels, thus degrading the adjacent channel leakage ratio (ACLR). The third kind of unwanted emissions are those emitted in the spurious domain, beyond the adjacent channel region which can seriously violate the given spurious emission limits [1], [4]–[6]. Furthermore, in FDD devices, the generated spurious components can also overlap with the device's own receive band, causing receiver desensitization [1], [7]–[9], as demonstrated in Fig. 1

In the recent literature, there have been some works on efficient concurrent digital predistortion (DPD) techniques for CA transmitters that employ only a single PA [3], [10]–[16]. These works assume that the CCs are separated by a relatively large distance such that the spurious emissions are filtered out by the transmit RF filter, and hence linearization of only the main carriers is pursued. The advantage of such concurrent DPD techniques is the reduced sampling rates of both the DAC and ADC in the DPD system, compared to conventional full-band DPD which linearizes the whole aggregated spectrum at a significantly higher sampling rate. However, most of the concurrent DPD techniques developed so far are based on the indirect learning architecture (ILA) when it comes to the DPD parameter estimation, which requires the observation of both CCs at the same time in order to compute the post inverse solution, thus calling for two feedback receivers for proper DPD operation [3], [10]–[12].

Manuscript received January 17, 2017. Mahmoud Abdelaziz, Lauri Anttila, Adnan Kiayani, and Mikko Valkama are with the Laboratory of Electronics and Communications Engineering, Tampere University of Technology, Tampere, Finland.

This work was supported by the Finnish Funding Agency for Technology and Innovation (Tekes) under the project "Future Small-Cell Networks using Reconfigurable Antennas (FUNERA)", and by the Linz Center of Mechatronics (LCM) in the framework of the Austrian COMET-K2 programme. The work was also funded by Tekes, Nokia Bell Labs, Huawei Technologies Finland, TDK-EPCOS, Pulse Finland and Sasken Finland under the 5G TRx project, and by the Academy of Finland under the projects 288670 "Massive MIMO: Advanced Antennas, Systems and Signal Processing at mm-Waves", 284694 "Fundamentals of Ultra Dense 5G Networks with Application to Machine Type Communication", and 301820 "Competitive Funding to Strengthen University Research Profiles".

In this paper, a novel reduced-complexity concurrent DPD solution with a *single feedback receiver* is proposed for dual-band transmitters. The proposed DPD main path processing is based on modeling and injecting the unwanted emissions within and around the main CCs into the PA input with opposite phase, such that the unwanted inband and adjacent channel emissions are canceled at the PA output. The parameter learning is based on a closed-loop feedback system, instead of ILA, with a very simple decorrelation-based learning rule, which aims to minimize the correlation between the nonlinear distortion observed at the PA output (per CC) and specific locally generated baseband nonlinear basis functions. This enables learning the DPD parameters separately for each CC, utilizing only a single feedback receiver.

There have been some recent research efforts in the existing literature utilizing only a single feedback receiver for parameter estimation in the concurrent DPD context [14]–[16]. In all these solutions, however, the PA behavioral model has to be extracted first and then used in the ILA-based learning. Such extra step, which significantly adds to the learning complexity, is not required in the proposed DPD solution. Overall, like will be shown through detailed complexity comparison, the proposed decorrelation-based DPD learning is substantially less complex compared to the ILA-based learning, while offering similar or even slightly enhanced linearization performance.

In general, the decorrelation-based DPD learning was originally introduced by the authors in [17], [18] for mitigating the emissions at the spurious intermodulation (IM) sub-bands only (i.e., IM3, IM5, etc., sub-bands), while not considering the nonlinear distortion at and around the main carriers. Consequently, the EVM and ACLR degradations due to PA nonlinearity were not tackled at all in [17], [18]. The concurrent DPD solution proposed in this article is, in turn, specifically developed and tailored to mitigate the distortion at and around the main carriers.

Moreover, the proposed concurrent DPD can be complemented with the spurious domain DPD developed in [17], [18] to obtain a complete and highly flexible DPD structure which can target the unwanted emissions at any sub-band, whether at or around the main CCs or at any spurious domain IM sub-band, while using only a single feedback observation receiver. Such complete solution is very flexible in the sense that it allows for linearizing any sub-bands of choice, based on the target application and linearization requirements.

An alternative, flexible ILA-based concurrent DPD solution was also introduced in [19]. However, this solution requires significant extra processing in order to guide the DPD to linearize only the targeted sub-band(s). In particular, direct modeling at the sub-band(s) that we do not eventually seek to linearize, is required in [19]. Such extra processing step is not required in the solution proposed in this paper. Furthermore, in [20], a flexible full-band DPD solution, which optimizes the DPD coefficients to minimize the nonlinear distortion at a particular frequency or sub-band, was proposed. However, like other full-band DPD techniques, it requires very high sampling rates in the transmitter and feedback receiver when the carrier spacing between CCs increases. On the other hand, the proposed solution in this paper does not have such drawbacks.

The rest of this article is organized as follows: Section II presents the mathematical modeling of the nonlinear distortion in a practical dual-band scenario. Stemming from this nonlinear distortion model, the proposed concurrent DPD main path processing is formulated. Then, Section III presents the proposed concurrent DPD parameter learning solution, building on the closed-loop decorrelation approach. Section IV then presents an extended decorrelation-based DPD architecture where the main component carriers as well as any other harmful nonlinear distortion products at other sub-bands are suppressed. A detailed complexity analysis and comparison with state-of-the-art single feedback concurrent DPD techniques are then presented in Section V. Sections VI and VII report comprehensive simulation-based as well as practical RF measurement results of the proposed DPD solution, respectively, incorporating both LTE/LTE-Advanced base-station and user equipment side PAs. Finally, Section VIII summarizes the main findings of this article.

II. Nonlinearity Modeling and Proposed DPD Processing

In this section, the modeling of the nonlinear distortion at and around the main carriers is performed in a practical case of non-contiguous carrier aggregation with two component carriers. The basic processing of the proposed concurrent DPD is then formulated stemming from that model. In principle, the proposed DPD can also be generalized to more than two component carriers. However, we will limit the discussion in this paper to the two-component carrier scenario for the sake of presentation compactness. The Parallel Hammerstein (PH) PA model, with odd-order nonlinearities, is adopted in all the modeling and DPD developments, since it has been shown to accurately model the nonlinear behavior of various classes of real PAs [21]. However, we wish to emphasize that the proposed concurrent DPD is compatible with other PA behavioral models as well, e.g., the Volterra model [21].

A. Nonlinear Distortion Modeling around the Main Carriers

We perform the modeling at the composite baseband equivalent level, in which the frequency spacing between the two component carriers is assumed to be $2f_{IF}$. A separate direct conversion TX chain is assumed per CC, and thus in the considered TX architecture, there is no IF upconversion, while the notation f_{IF} simply refers in this manuscript to half the carrier spacing between the two CCs at RF.

Assuming a P^{th} order PH PA model, with monomial nonlinearities and FIR branch filters, the composite baseband equivalent signals at the PA input and output, respectively, read

$$x(n) = x_1(n)e^{j2\pi\frac{f_{IF}}{f_s}n} + x_2(n)e^{-j2\pi\frac{f_{IF}}{f_s}n}, \tag{1}$$

$$y(n) = \sum_{\substack{p=1 \\ p,\ \text{odd}}}^{P} f_{p,n} \star |x(n)|^{p-1}x(n), \tag{2}$$

where $x_1(n)$ and $x_2(n)$ denote the baseband component carrier signals, $f_{p,n}$ denotes the p^{th} order PH branch filter impulse response, and $\star$ is the convolution operator.

The baseband equivalent distortion terms at and around the main CCs can be extracted by the direct substitution of (1) in (2), which yields

$$y_{\pm}(n) = \sum_{\substack{p=1 \\ p,\ \text{odd}}}^{P} f_{\pm,p,n} \star u_{\pm,p}(n), \tag{3}$$

where $f_{\pm,p,n}$ denote the baseband equivalent impulse responses corresponding to the wideband PH PA model filters $f_{p,n}$, evaluated around $x_1(n)$ and $x_2(n)$ respectively, and defined as

$$f_{\pm,p,n} = h_{P,n}^{LPF} \star \{e^{\mp j2\pi \frac{f_{IF}}{f_s} n} f_{p,n}\}, \tag{4}$$

with $h_{P,n}^{LPF}$ denoting an ideal low pass filter with passband width P times the bandwidth of the wider component carrier. Meanwhile, $u_{\pm,p}(n)$ in (3) denote the corresponding p^{th} order static nonlinear (SNL) basis functions, related to the nonlinear distortion around $x_1(n)$ and $x_2(n)$, respectively. Assuming a ninth-order PA model (i.e., $P = 9$), the SNL basis functions representing the nonlinear distortion around the first CC $x_1(n)$, as a concrete example, read

$$u_{+,1}(n) = x_1 \tag{5}$$

$$u_{+,3}(n) = x_1|x_1|^2 + 2x_1|x_2|^2 \tag{6}$$

$$u_{+,5}(n) = x_1|x_1|^4 + 3x_1|x_2|^4 + 6x_1|x_1|^2|x_2|^2 \tag{7}$$

$$u_{+,7}(n) = x_1|x_1|^6 + 4x_1|x_2|^6 + 12x_1|x_1|^4|x_2|^2 + 18x_1|x_1|^2|x_2|^4 \tag{8}$$

$$u_{+,9}(n) = x_1|x_1|^8 + 5x_1|x_2|^8 + 20x_1|x_1|^6|x_2|^2 + 40x_1|x_1|^2|x_2|^6 + 60x_1|x_1|^4|x_2|^4 \tag{9}$$

The time index (n) has been excluded from $x_1(n)$ and $x_2(n)$ in (5)-(9) only to simplify the presentation. Similarly, the corresponding basis functions for the second CC x_2 (i.e., $u_{-,p}(n)$) can be obtained by interchanging x_1 and x_2 in the above expressions. It is worth mentioning that similar basis function expressions have been developed in [22] but up to seventh order nonlinearity only. Moreover, in [22] these basis functions were presented as a simplification of the basis functions in [10] without assuming a particular PA model with memory. In this work, we thus show that (5)-(9) represent the exact basis functions when a PH PA model is assumed. Next, the behavioral model in (3)-(9) is utilized to formulate the proposed injection based concurrent DPD concept, specifically tailored to suppress the distortion at and around the main carriers.

B. Proposed Concurrent DPD Processing

Since we are mostly concerned with the nonlinear distortion at and around the main carriers, we first rewrite equation (3) to separate the linear part from the nonlinear terms as

$$y_{\pm}(n) = f_{\pm,1,n} \star u_{\pm,1}(n) + \sum_{\substack{p=3 \\ p,\ \text{odd}}}^{P} f_{\pm,p,n} \star u_{\pm,p}(n). \tag{10}$$

The main idea of the proposed concurrent DPD processing is then to inject an additional low-power cancellation signal, with similar structure to the nonlinear terms in (10), into the PA input, such that the nonlinear distortion at and around the main carriers is mitigated at the PA output. Therefore, we can obtain an appropriate digital injection signal, to mitigate the nonlinear distortion terms around $x_1(n)$, by adopting the SNL basis functions $u_{+,p}(n)$, $p > 1$, in (6)-(9), combined with a proper bank of DPD filters $\alpha_{+,p,n}$. Similarly, an additional digital injection signal can be applied at the PA input to mitigate the nonlinear distortions around $x_2(n)$ by applying another bank of DPD filters $\alpha_{-,p,n}$ together with the SNL basis functions $u_{-,p}(n)$. This flexibility in operation is one advantage of the proposed DPD principle, since it is not necessarily required in all scenarios to mitigate the distortions around both CCs. For example, the EVM and/or ACLR requirements can be, in general, different between the two CCs, and thus only one of the two CCs might need predistortion. This flexibility can reduce power consumption, which is especially important for small devices.

In general, incorporating such concurrent DPD processing for both main carriers $x_1(n)$ and $x_2(n)$ with polynomial order Q, the composite baseband equivalent PA input signal reads

$$\tilde{x}(n) = x(n) + \left(\sum_{\substack{q=3 \\ q,\ \text{odd}}}^{Q} \alpha_{+,q,n}^{*} \star u_{+,q}(n) \right) e^{j2\pi \frac{f_{IF}}{f_s} n} + \left(\sum_{\substack{q=3 \\ q,\ \text{odd}}}^{Q} \alpha_{-,q,n}^{*} \star u_{-,q}(n) \right) e^{-j2\pi \frac{f_{IF}}{f_s} n} \tag{11}$$

We use $\tilde{(.)}$ variables here, and in the continuation, to indicate DPD processing and the corresponding predistorted signals. Notice that while the polynomial order Q in (11) is assumed identical for both CCs, mainly for notational simplicity, it can easily be set also independently in practice for the two CCs if, e.g., the linearization performance is to be tailored in a per CC manner. Furthermore, the achievable mitigation of the nonlinear distortion around the main carriers depends directly on the estimation and optimization of the concurrent DPD filter coefficients $\alpha_{\pm,q,n}$. This is addressed in detail in the next section. It is also to be noted that the linear basis function in (5) is not used in the proposed DPD, which reduces the required number of DPD coefficients. Thus, both the DPD learning and main path complexities are reduced. The reason for not including (5) is that the primary objective of the DPD is to mitigate the nonlinear distortions only, while the linear distortions can be considered part of the overall communications channel, which is always equalized at the receiver side. Meanwhile, the concurrent DPD solutions in [3], [10]–[16] utilize the ILA, which requires using the linear term for a correct post-inverse estimation.

III. Closed-Loop Parameter Learning Using the Decorrelation Principle

In this section, we build upon the previous nonlinear distortion modeling and the proposed concurrent DPD processing in order to formulate a highly efficient and computationally

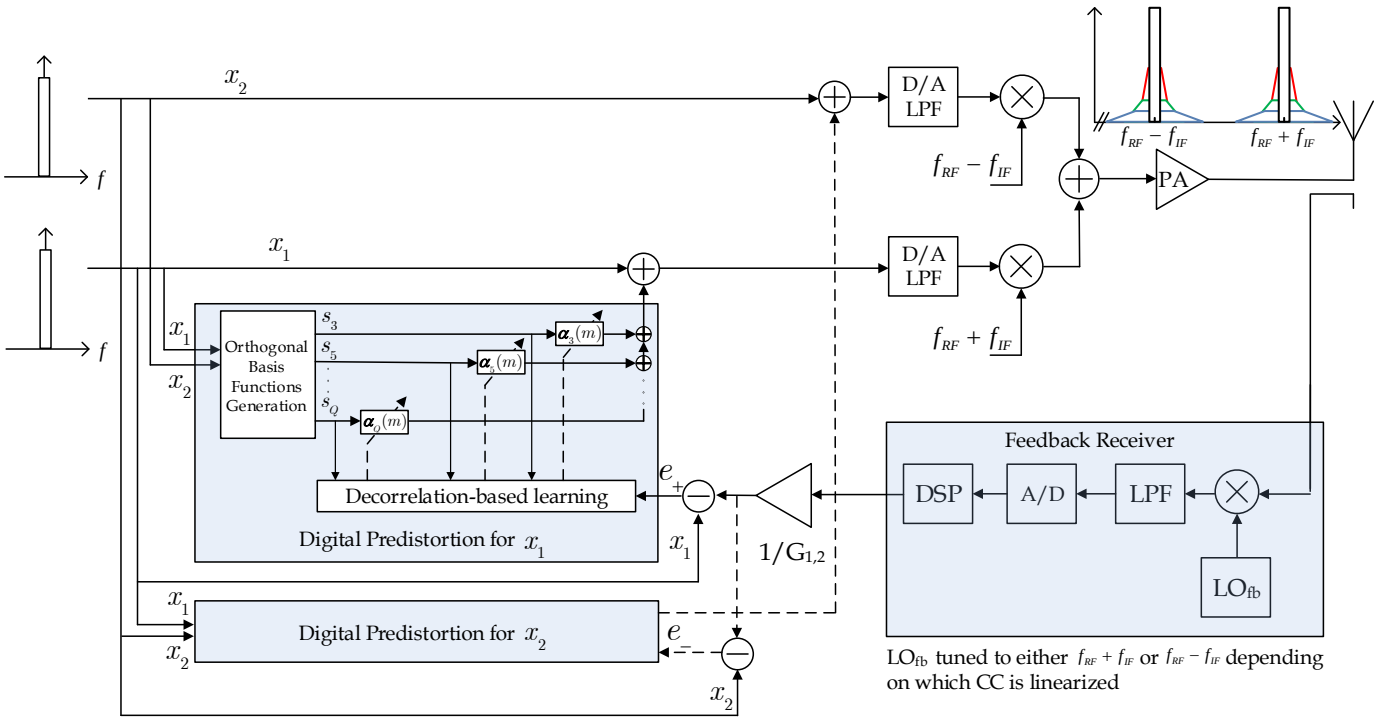

Fig. 2. Block diagram of the adaptive decorrelation-based concurrent DPD adopting closed-loop learning with a single feedback observation receiver. The PA distortion is observed in a per-CC manner and the DPD coefficients $\boldsymbol{\alpha}_q(m)$ of a given CC are adaptively estimated using the decorrelation-based learning rule. The orthogonalized basis functions s_q representing the nonlinear distortion at the considered CC are filtered with the corresponding DPD coefficients and then injected at the PA input. This process is iterated, per CC, until the coefficients converge to the desired value at which the correlation between the PA observation and the basis function samples is minimized.

feasible closed-loop estimation algorithm for learning the concurrent DPD filter coefficients, based on the decorrelation principle. We formulate the DPD parameter optimization task here as minimizing the correlation between the nonlinear distortion at and around the considered main carrier, and the basis functions representing the nonlinear distortion.

The DPD learning is performed one carrier at a time, while utilizing only a single feedback receiver. On one hand, this requires twice the learning time when compared to the dual feedback approach. On the other hand, the PA characteristics usually vary in the order of seconds or tens of seconds [23]. This is much slower than the DPD learning time which is in the order of milliseconds, as demonstrated in Section VI, which means that such per-CC learning is well justified.

In order to extract the nonlinear distortion around each of the main carriers, the useful or linear signal components have to be properly subtracted from the observations at the PA output. This requires an estimate of the complex linear gain of the PA, per CC, which can easily be obtained using simple linear estimation techniques (e.g., least squares). The baseband equivalent nonlinear distortion terms, denoted by $e_{\pm}(n)$ at the PA output around $x_1(n)$ and $x_2(n)$, respectively, can then be calculated as follows

$$e_+(n) = h_{Q,n}^{LPF} \star \{y(n)e^{-j2\pi\frac{f_{IF}}{f_s}n}\}/G_1 - x_1(n) \qquad (12)$$

$$e_-(n) = h_{Q,n}^{LPF} \star \{y(n)e^{j2\pi\frac{f_{IF}}{f_s}n}\}/G_2 - x_2(n), \qquad (13)$$

where G_1 and G_2 are the estimated complex linear gains of the PA for $x_1(n)$ and $x_2(n)$, respectively, while $h_{Q,n}^{LPF}$ denotes the lowpass filtering impulse response of the feedback receiver chain with a passband width of Q times the bandwidth of the wider CC.

The next step is to locally generate the combined basis functions in (6)-(9) and their delayed replicas, and apply the decorrelation-based learning principle. As the name indicates, the learning is based on finding the DPD filter coefficients $\alpha_{\pm,q,n}$ in (11) that minimize the correlation between the extracted nonlinear distortion at the PA output, given in (12) and (13), and the locally generated basis functions, as also illustrated in Fig. 2.

In general, the basis functions in (5)-(9) are mutually correlated and thus a basis function orthogonalization procedure is required in order to have a faster and smoother convergence of the DPD parameter estimates during the learning process, as well as better numerical properties for hardware implementation [24]. In principle, any suitable orthogonalization procedure can be adopted, e.g., Gram-Schmidt, QR or singular value decomposition based, or using a lower complexity iterative orthogonalization algorithm [25]. The orthogonalized versions of the SNL basis functions $u_{\pm,q}(n)$ are denoted in the following by $s_{\pm,q}(n)$.

Then, assuming a DPD filter memory order of N_q per each of the new orthogonal basis functions $s_{\pm,q}(n)$, and an estimation block size of M samples, we combine all the samples and the corresponding DPD filter coefficients, within

processing block m, into the following vectors and matrices:

$$\mathbf{s}_{\pm,q}(n_m) = [s_{\pm,q}(n_m) \; ... \; s_{\pm,q}(n_m - N_q)], \quad (14)$$

$$\mathbf{S}_{\pm,q}(m) = [\mathbf{s}_{\pm,q}(n_m)^T \; ... \; \mathbf{s}_{\pm,q}(n_m + M - 1)^T]^T, \quad (15)$$

$$\mathbf{S}_{\pm}(m) = [\mathbf{S}_{\pm,3}(m) \; \mathbf{S}_{\pm,5}(m) \; ... \; \mathbf{S}_{\pm,Q}(m)], \quad (16)$$

$$\boldsymbol{\alpha}_{\pm,q}(m) = [\alpha_{\pm,q,0}(m) \; \alpha_{\pm,q,1}(m) \; ... \; \alpha_{\pm,q,N_q}(m)]^T, \quad (17)$$

$$\bar{\boldsymbol{\alpha}}_{\pm}(m) = [\boldsymbol{\alpha}_{\pm,3}(m)^T \; \boldsymbol{\alpha}_{\pm,5}(m)^T \; ... \; \boldsymbol{\alpha}_{\pm,Q}(m)^T]^T, \quad (18)$$

where n_m denotes the index of the first sample within block m. The block-adaptive decorrelation-based DPD coefficient update, with learning rate μ, then reads

$$\bar{\boldsymbol{\alpha}}_{\pm}(m+1) = \bar{\boldsymbol{\alpha}}_{\pm}(m) - \mu \, [\mathbf{e}_{\pm}(m)^H \mathbf{S}_{\pm}(m)]^T, \quad (19)$$

where $\mathbf{e}_{\pm}(m) = [e_{\pm}(n_m) \; ... \; e_{\pm}(n_m + M - 1)]^T$ and $\mathbf{S}_{\pm}(m)$ denote the error signal vector and the filter input data matrix, respectively, all within the processing block m. The updated DPD coefficients $\bar{\boldsymbol{\alpha}}_{\pm}(m+1)$ are then used to filter the next block of M samples, and the process is iterated until convergence. The DPD parameter update interval can be chosen to be L samples, with $M \leq L$. This adds more flexibility to the proposed solution, and allows for tolerating arbitrarily long loop delays through the proper selection of M and L. This, in turn, facilitates stable operation under various hardware and software processing latency constraints, as demonstrated in [26] in the context of DPD for spurious emissions mitigation at the IM sub-bands. In general, this computing-efficient coefficient learning approach has been observed, in both simulations and RF measurements, to be stable and to converge reliably assuming that the step-size μ is chosen properly.

IV. Extended DPD solution and Feedback Receiver Aspects

A. Decorrelation-based DPD solution for all sub-bands

In this section, an extended decorrelation-based sub-band DPD solution is presented. It combines the processing developed in the previous sections for concurrent linearization, and the authors' earlier work in [18] for spurious domain linearization. Such complete sub-band DPD solution has the capability to suppress nonlinear distortion in non-contiguous CA/multi-band transmitters in a flexible and efficient manner, at and around the main carriers as well as in the spurious domain, using the decorrelation-based learning rule and a single feedback receiver operating at a lower sample rate. The leading principle in the parameter learning is to minimize the correlation between the distortion at the main CCs, and/or at any of the IM sub-bands, and specific low-rate baseband SNL basis functions representing the nonlinear distortion at the corresponding sub-bands. The SNL basis functions representing the nonlinear distortion at the IM sub-bands were already derived in [18], and are denoted by $u_{b\pm,q}(n)$, where $b = 3, 5, ..., B$ is the sub-band index (i.e., $b = 3$ for the IM3 sub-bands, $b = 5$ for the IM5 sub-bands, etc.).

Incorporating now the sub-band DPD processing with DPD polynomial order Q, and aggregating at the same time the linearization processing at all sub-bands simultaneously, the composite baseband equivalent PA input signal, assuming that $Q \geq B$, reads then

$$\begin{aligned}\tilde{x}(n) = x(n) &+ \left(\sum_{\substack{q=3 \\ q,\ \text{odd}}}^{Q} \alpha^*_{+,q,n} \star s_{+,q}(n) \right) e^{j2\pi \frac{f_{IF}}{f_s} n} \\ &+ \left(\sum_{\substack{q=3 \\ q,\ \text{odd}}}^{Q} \alpha^*_{-,q,n} \star s_{-,q}(n) \right) e^{-j2\pi \frac{f_{IF}}{f_s} n} \\ &+ \sum_{\substack{b=3 \\ b,\ \text{odd}}}^{B} \left(\sum_{\substack{q=b \\ q,\ \text{odd}}}^{Q} \alpha^*_{b+,q,n} \star s_{b+,q}(n) \right) e^{j2\pi \frac{b \times f_{IF}}{f_s} n} \\ &+ \sum_{\substack{b=3 \\ b,\ \text{odd}}}^{B} \left(\sum_{\substack{q=b \\ q,\ \text{odd}}}^{Q} \alpha^*_{b-,q,n} \star s_{b-,q}(n) \right) e^{-j2\pi \frac{b \times f_{IF}}{f_s} n}\end{aligned} \quad (20)$$

where $s_{b\pm,q}(n)$ are the q^{th} order orthogonalized versions of the SNL basis functions $u_{b\pm,q}(n)$ at the b^{th} sub-band, and $\alpha_{b\pm,q,n}$ are the corresponding DPD filters to be estimated using the block-adaptive learning solution which will be described next. Notice that, in (20), for notational simplicity, the DPD orders at different sub-bands are assumed to be identical, while in reality they can easily be set independently based on the corresponding linearization requirements.

The block-adaptive decorrelation-based DPD coefficient update for the b^{th} sub-band reads

$$\bar{\boldsymbol{\alpha}}_{b\pm}(m+1) = \bar{\boldsymbol{\alpha}}_{b\pm}(m) - \mu \, [\mathbf{e}_{b\pm}(m)^H \mathbf{S}_{b\pm}(m)]^T, \quad (21)$$

where $\mathbf{S}_{b\pm}(m)$ and $\bar{\boldsymbol{\alpha}}_{b\pm}(m)$ are defined as in (16) and (18), using the orthogonalized basis functions corresponding to the b^{th} sub-band. The error signal vector is denoted by $\mathbf{e}_{b\pm}(m) = [e_{b\pm}(n_m) \; ... \; e_{b\pm}(n_m + M - 1)]^T$. For $b = 1$, $e_{\pm}(n)$ are defined in (12) and (13), while for the IM sub-bands $b = 3, 5, ..., B$, $e_{b\pm}(n) = \tilde{y}_{IMb_{\pm}}(n)$, which denotes the baseband equivalents of the PA output at the b^{th} sub-bands, with the corresponding sub-band DPD processing included adopting the current coefficients, $\bar{\boldsymbol{\alpha}}_{b\pm}(n)$. In other words, at the actual IM sub-bands, the error signal in the learning is directly the observed PA output since the ideal linear signal term is, by definition, zero.

Thus, as we can see from (21), the DPD learning for all the sub-bands including the main carriers is adopting the simple decorrelation principle. And since the learning is done one sub-band at a time, a single computing engine or correlator can be reused in the actual hardware implementation for the different sub-bands. This learning scheme thus provides a very simple, cost-effective, and high performance solution, as will also be demonstrated through the simulations and RF measurement results in Sections VI and VII, respectively.

TABLE I
DPD MAIN PATH PROCESSING COMPUTATIONAL COMPLEXITY COMPARISON. THE OVERSAMPLING FACTOR $R = Q$ WITHOUT FILTERED BASIS FUNCTIONS, AND $R < Q$ WITH FILTERED BASIS FUNCTIONS.

	BF generation (FLOP/sample)	BF extra filtering, if $R < Q$ (FLOP/sample)	DPD main path processing (FLOP/sample)	Minimum processing sample rate (Msps)
1-Full-band DPD	$Q + 2$	$\sum_{q=3}^{Q}[4N_b + 2]R/q$	$(Q + 1)(4N + 3)$	$R(W_1 + W_2 + \Delta f)$
2-[10]	$6 + 4\sum_{q=3}^{Q} q$	$2\sum_{q=3}^{Q}[4N_b + 2]R/q$	$2(Q + 1)(4N + 3)$	$R \times max(W_1, W_2)$
3-[14], [15]	$6 + 4\sum_{q=3}^{Q} q$	$2\sum_{q=3}^{Q}[4N_b + 2]R/q$	$2(Q + 1)(4N + 3)$	$R \times max(W_1, W_2)$
4-[16]	$Q + 2$	$2\sum_{q=3}^{Q}[4N_b + 2]R/q$	$(Q + 1)(4N + 3) + 2(5N_s + 6)$	$R(W_1 + W_2)$
5-This work	$6 + 4\sum_{q=3}^{Q} q$	$2\sum_{q=3}^{Q}[4N_b + 2]R/q$	$2(Q - 1)(4N + 3)$	$R \times max(W_1, W_2)$

TABLE II
DPD LEARNING COMPLEXITY COMPARISON.

	PA estimation (FLOP/M samples)	BF generation (FLOP/KM samples)	DPD estimation (FLOP/KM samples)	Minimum learning sample rate (Msps)
1-Full-band DPD One feedback RX	0	$KM[Q + 2]$	$4K[(M + (Q + 1)(N + 1)/6) \times (Q + 1)^2(N + 1)^2/4]$	$R(W_1 + W_2 + \Delta f)$
2-[10] Two feedback RXs	0	$KM[6 + 4\sum_{q=3}^{Q} q]$	$4K[(M + (Q + 1)(N + 1)/3) \times (Q + 1)^2(N + 1)^2]$	$R \times max(W_1, W_2)$
3-[14], [15] One feedback RX	$4[(M + (Q + 1)(N + 1)/3) \times (Q + 1)^2(N + 1)^2] + 8M(Q + 1)(N + 1) - 2M$	$KM[6 + 4\sum_{q=3}^{Q} q]$	$4K[(M + (Q + 1)(N + 1)/3) \times (Q + 1)^2(N + 1)^2]$	$R \times max(W_1, W_2)$
4-[16] One feedback RX	$4[(M + (Q + 1)(N + 1)/6) \times (Q + 1)^2(N + 1)^2/4] + 4M(Q + 1)(N + 1) - 2M$	$KM[Q + 2]$	$4K[(M + (Q + 1)(N + 1)/6) \times (Q + 1)^2(N + 1)^2/4]$	$R(W_1 + W_2)$
5-This work One feedback RX	$16M - 4$	0	$4K[(2M + 1)(Q - 1)(N + 1) - M]$	$R \times max(W_1, W_2)$

B. Decorrelation-based DPD Solution for Single CC/Band Scenarios

The same decorrelation-based DPD learning algorithm can be used, not only in the earlier considered dual carrier/band scenarios, but also in more classical single CC/band transmitters. This can be achieved by simply setting $x_2(n) = 0$ in (6)-(9), and thus $x_1(n)$ becomes the main/only carrier of interest. The decorrelation-based learning can then minimize the correlation between the single CC -based basis functions and the nonlinear distortion around the main carrier $x_1(n)$ using the same learning rule as explained earlier, while setting $f_{IF} = 0$. This single CC mode of operation can also be used when the carrier spacing between the two CCs gets narrower, by interpreting the composite baseband signal as one arbitrary baseband waveform centered at zero frequency. This approach naturally assumes that the sample rate for processing the composite signal as a whole is still feasible, implying then also that all sub-bands are processed and linearized simultaneously. This further emphasizes the flexibility of the proposed DPD solution for different transmission scenarios and system aspects. In this context, it is also worth mentioning that the work in [27] proposes a concurrent DPD for scenarios in which the CCs are narrowly spaced. This approach uses a multiple-input multiple-output Volterra DPD structure with filtered basis functions, thus reducing the sample rates required by the DAC and ADC in the DPD system.

C. DPD Feedback Receiver Aspects

In order to further reduce the complexity of the proposed DPD with Q^{th} order DPD processing, a narrower BW feedback receiver can be used even when higher-order nonlinearities are included in the estimation and linearization processing. In other words, the feedback receiver sample rate of a Q^{th} order DPD can be chosen to be R times the BW of the wider linearized CC, where $R < Q$. As an example, in a dual carrier scenario, if the BW of each CC is 20 MHz, and a ninth-order ($Q = 9$) concurrent DPD is adopted, the observed PA output can be filtered such that only, e.g., 60 MHz is captured per CC (i.e., $R = 3$), instead of $9 \times 20 = 180$ MHz. This can further reduce the complexity of the feedback receiver in the proposed DPD architecture, in particular the feedback ADC, while still providing very good linearization performance, as will be shown in the RF measurement examples. Similarly, in the DPD main path processing, the SNL basis functions can be filtered to reduce the DPD sample rate and thus complexity, as will be described in more details in Section V. A similar idea, based on filtering the DPD basis functions, was also proposed in [28] as a way of reducing the DPD complexity in ordinary ILA-based DPD learning architectures.

V. COMPLEXITY ANALYSIS AND COMPARISON AGAINST STATE-OF-THE-ART

This section presents a detailed quantitative comparison between the complexities of the single feedback concurrent DPD proposed in this article, and the existing state-of-the-art single feedback concurrent DPDs in [14]–[16]. The complexities of the dual feedback concurrent DPD, as in [10], and the classical full-band DPD are also presented for reference. The number of floating point operations (FLOP) is used to

quantify the complexity of each DPD technique [21]. Moreover, both the DPD main path processing complexity and the parameter learning complexity are considered in the analysis and comparisons, as shown in Tables I and II, respectively. To the best of the authors' knowledge, this is the first time that such a comprehensive complexity analysis of the state-of-the-art single feedback concurrent DPD techniques is reported in the literature.

The following assumptions are made in all of the considered DPD techniques in order to ensure a fair comparison:

- A dual carrier scenario is considered, and the DPD is linearizing both CCs. A separate analog TX chain for each CC and a shared PA are assumed for generating the dual-carrier RF signal.
- In principle, any suitable nonlinear model can be used. However, for fairness of comparison, the basis functions derived in this work stemming from the PH PA model, in (5)-(9), are used in all the considered concurrent DPD techniques.
- A suitable orthogonalization processing is applied to the basis functions in all the considered techniques for better numerical properties and stability in the DPD parameter estimation [29], [30]. The complexity of the orthogonalization process is identical in all cases and is thus excluded in the analysis.
- Proper synchronization is required between the PA output observation and the baseband basis function samples in all methods, and thus the synchronization complexity is also excluded from the comparison. However, it is worth mentioning that some extra effort is required for synchronization in the methods proposed in [14], [15] when compared to the other considered methods, as explained in [14].

The notations used in the complexity analysis are consistent with the notations throughout the paper, along with some additional symbols that are all summarized here: Q denotes the DPD nonlinearity order. N denotes the DPD filter memory order, where it is assumed that each q^{th} order DPD filter $\alpha_{\pm,q,n}$ has $N+1$ memory taps, for simplicity. M denotes the estimation block size in both the block-adaptive filtering used in this work, as well as the block LS estimation. K denotes the number of block-adaptive iterations in this work, as well as the number of ILA iterations in ILA-based DPD learning. W_1, W_2, denote the bandwidths of the first and second CCs respectively, while the carrier spacing is denoted with Δf. Finally, N_s denotes the memory depth of the filters used in [16] for carrier separation and relocation before transmitting each CC on separate TX chains. These filters are assumed to be FIR filters with symmetrical coefficients.

In case of applying additional filtering to the basis functions (BFs) to reduce the DPD processing sample rate, as explained in Section IV-C, the symbol R denotes the amount of oversampling applied in the basis functions generation compared to the original CC bandwidths W_1 and W_2. In the normal scenario without filtered BFs, this oversampling factor $R = Q$, otherwise $R < Q$. N_b denotes the memory depth of the BF bandlimitation filter used for filtering the basis functions, which is assumed to be a computationally efficient polyphase FIR decimator structure [31].

The results of the complexity analysis are presented in Tables I and II, with the main findings being the following:

- The DPD main path processing complexity of the solution developed in this work is lower than in any of the other techniques. This is because the proposed DPD solution does not require processing of the linear basis function, opposed to all other methods, as explained in Section II. This is reflected on the third column of Table I.
- When compared to the single feedback concurrent DPD in [16], the proposed DPD has significantly lower main path complexity, despite having greater basis function generation complexity. In [16], a single DPD is used for both CCs, resulting in a higher DPD sample rate. Moreover, two carrier separation and relocation filters are required in [16] to transmit the aggregated carriers on separate TX chains, thus adding to the overall DPD running complexity. These aspects are reflected on the first, third, and fourth columns of Table I.
- The single feedback concurrent DPDs in [14]–[16] require PA direct model extraction, which significantly adds to the DPD learning complexity. On the other hand, in this work only the linear gain of the PA is required, implying substantially lower complexity. This is reflected on the first column of Table II.
- The same basis function samples used in the DPD main path processing can be reused in the decorrelation-based DPD learning in this work, as illustrated in Fig. 2. This is not possible in the other DPD solutions due to the nature of the ILA-based learning which requires a post-inverse estimation whose basis functions are generated from the PA output samples. This is an important difference and is reflected on the second column of Table II.
- DPD parameter estimation developed in this work is significantly less complex than the other methods, which are all ILA-based. This is reflected on the third column of Table II.

Concrete numerical examples of the overall main path processing complexity, in terms of FLOP per second, as well as the learning complexity in terms of FLOP per learning procedure, will be provided in the next section, together with the corresponding linearization performance results.

VI. Simulation Results

In this section, practical carrier aggregation based simulation studies, using a real PA model, are reported in order to quantitatively compare the complexity and performance of the proposed decorrelation-based concurrent DPD and state-of-the-art concurrent DPD methods mentioned in Section V. Both the inband waveform purity and the adjacent channel leakage due to spectral regrowth are quantified using the well-known EVM and ACLR metrics. [4], [32].

The considered dual carrier example is shown in Fig. 3 with two 10 MHz OFDM carriers and 100 MHz carrier spacing. A ninth-order PH PA model is used whose parameters have been identified using RF measurements with a true mobile PA transmitting at +22 dBm. This mobile PA has 29 dB gain, and +31

TABLE III
COMPLEXITY AND PERFORMANCE COMPARISON WITH STATE-OF-THE-ART CONCURRENT DPD METHODS

	Overall DPD complexity					DPD performance of CC1	
	Main path processing (GFLOP/s)	Overall learning complexity (MFLOP)	DPD sample rate (Msps)	Num. of est. samples	Num. of fb. RXs	EVM (%)	ACLR L / R (dBc)
Without DPD	0	0	N/A	N/A	N/A	4.01	35.52 / 36.19
1-Full-band DPD	238.59	108.6	990	30k	1	0.52	53.91 / 51.86
2-[10]	28.98	114	90	30k (per CC)	2	0.53	53.45 / 51.53
3-[14], [15]	28.98	152.4	90	40k (per CC)	1	0.53	53.45 / 51.53
4-[16]	113.94	146.4	180	40k (per CC)	1	0.52	53.00 / 51.55
5-This work	25.02	18.96	90	100k (per CC)	1	0.53	53.87 / 51.64

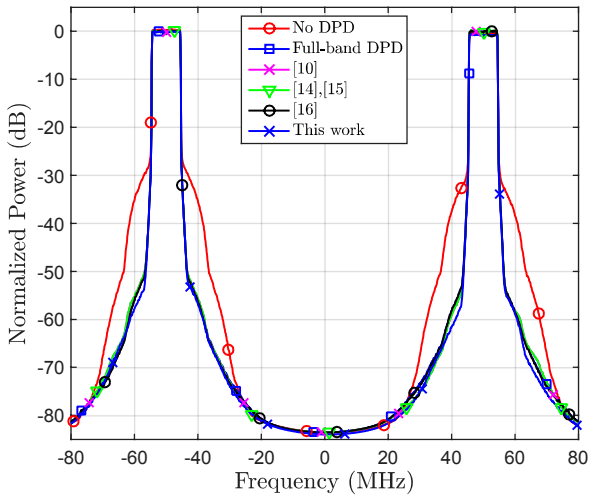

Fig. 3. Normalized PA output spectra of a concurrent noncontiguous intraband CA transmitter with two 10 MHz OFDM carriers with 100 MHz spacing, and 16-QAM subcarrier modulation. The PAPR is 12.5 dB. A ninth-order PH model is used. The PA parameters have been identified using RF measurements with a true mobile PA transmitting at +22 dBm.

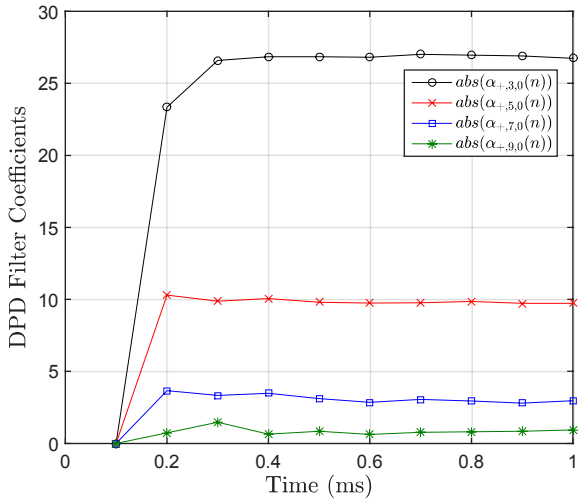

Fig. 4. Example convergence of the first memory taps, per basis function, of the ninth-order decorrelation-based CC1 DPD using a single realization of two 10 MHz OFDM carriers with 100 MHz spacing, and 16-QAM subcarrier modulation. A single learning block corresponds to 0.1 ms in real-time. The ninth-order PA parameters have been identified using RF measurements with a true mobile PA transmitting at +22 dBm.

dBm 1 dB compression point. The adopted parameterizations of the different DPD solutions are as follows: The estimation block size $M = 10k$ samples, and the DPD nonlinearity order $Q = 9$ in all the considered DPD methods. The number of block-adaptive iterations $K = 10$ in the proposed DPD, while the number of ILA iterations $K = 3$ in all the other considered DPD methods. In [10], [14], [15] and in the proposed DPD, the DPD memory order $N = 2$ per CC. Meanwhile, in [16] and in the full-band DPD the two CCs are predistorted with a single DPD, and thus a higher DPD memory order $N = 5$ is used. No filtering of the basis functions is performed in this comparison (i.e., $N_b = 0$). Additionally, in [16], $N_s = 50$.

All the considered DPD methods have almost the same linearization performance as shown in Fig. 3 and in Table III. However, the complexity is clearly in favor of the proposed concurrent DPD solution, showing a notable advantage in both the DPD main path processing complexity and learning complexity. The main path complexity is measured in GFLOP per second (GFLOP/s), while the learning complexity is measured in terms of the overall number of FLOP used in the learning process. The main findings of the complexity comparison in Table III can be summarized as follows: (*i*) The proposed DPD has clearly the lowest main path complexity in GFLOP/s. (*ii*) The number of samples used for DPD coefficients estimation is higher in the proposed DPD compared to the other considered DPD methods, which implies longer learning time. However, the time required for obtaining the correct DPD coefficients, per CC, in the proposed DPD is roughly 0.5 ms which is still very fast compared to the rate of change that can occur in the PA behavior [23], as shown in Fig. 4 for CC1 DPD coefficients. (*iii*) The overall learning complexity of the proposed DPD is significantly lower than all the other considered DPD methods despite using somewhat more samples.

VII. RF MEASUREMENT RESULTS

In this section, we provide results of comprehensive RF measurements using three commercially available power amplifiers, shown in Fig. 5. The first is an LTE-A band 1 base station (BS) PA, and the second is a general purpose wideband PA, suitable for interband CA. The third is an LTE-A band 25 user equipment (UE) PA. The RF measurement examples quantify and demonstrate the performance of the proposed decorrelation-based DPD solution, while other state-of-the-art DPD methods, which are based on the ILA principle for learning, are also implemented for reference.

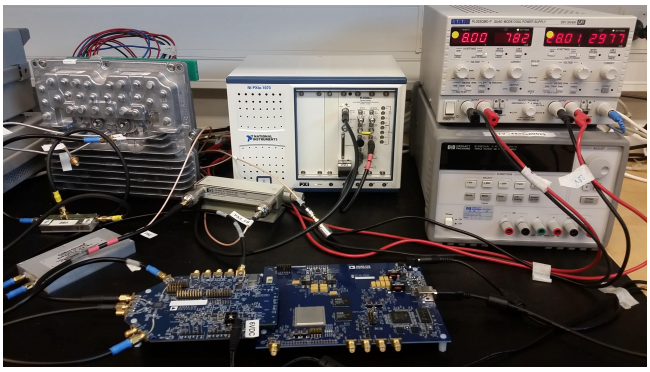

(a) Photo of the RF measurement setup

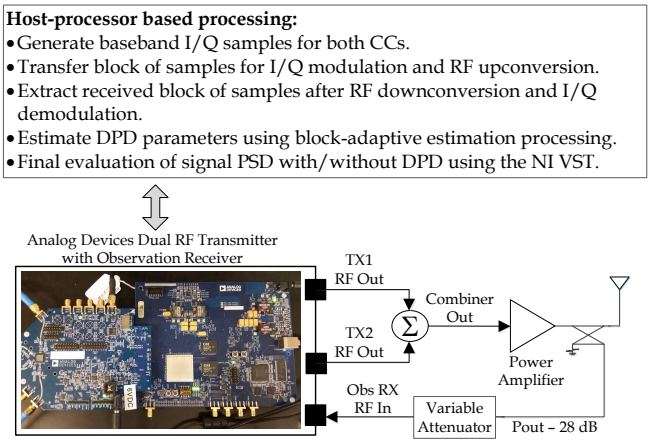

(b) Block diagram of the RF measurement setup

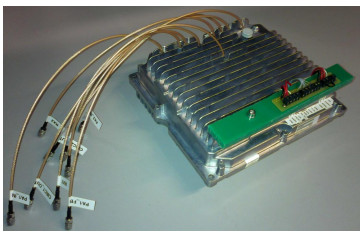

(c) LTE-A DL Band 1 (2110 MHz - 2170 MHz) basestation microwave PA

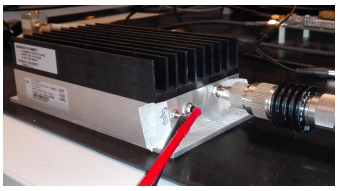

(d) Wideband microwave PA (10 MHz - 4200 MHz) suitable for LTE-A interband CA

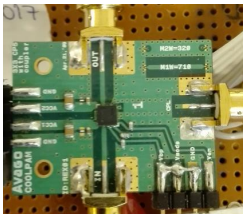

(e) LTE-A UL Band 25 (1850 MHz - 1915 MHz) UE microwave PA

Fig. 5. Hardware setup used in the RF measurements for testing and evaluating the proposed decorrelation-based concurrent DPD. The three RF power amplifiers used in the measurements are also shown.

A. RF Measurement Setup

The RF measurement setup is shown in Fig. 5. The Analog Devices evaluation board AD9368-2 has two RF transmitters, each with 250 MHz instantaneous bandwidth, that are used for implementing CA transmission scenarios. The board is also equipped with an observation receiver with 200 MHz instantaneous bandwidth, which is used as the DPD feedback receiver. The board is then connected to a host processor, which implements the baseband signal processing necessary for DPD, as well as the basic baseband waveform processing for the CCs. The digital baseband waveforms of the component carriers are divided into blocks of size $M = 10k$ samples each, which are first generated locally on the host processor, and then transferred to the evaluation board to perform RF I/Q modulation at the desired power level at the PA input. In the noncontiguous CA scenarios, the RF outputs of the two TX chains are combined using an RF combiner, and then connected to the input port of the external power amplifier. The PA output is then extracted via a directional coupler with 28 dB attenuation, and fed to the input of the evaluation board observation receiver, as illustrated also in Fig. 5. An extra variable attenuator is used to adjust the signal power at the directional coupler output to a level suitable for the observation receiver input. The observation receiver performs RF I/Q demodulation to bring the signal back to baseband, which is then used for the DPD learning. In all our measurement examples, the linear gain of the overall RF path, including the external PA and the attenuator, is estimated using block LS in order to be able to extract the nonlinear distortion at the PA output.

The DPD parameters used in the RF measurements are defined as follows: The estimation block size $M = 10k$ samples, and the DPD nonlinearity order $Q = 9$ in all the considered DPD methods. The number of block-adaptive iterations $K = 10$ in the proposed DPD solution, while the number of ILA iterations is $K = 3$ in all the other considered ILA-based reference DPD methods. In [10], [14], [15] and in the proposed DPD, the DPD memory order $N = 1$ per CC (i.e., two taps per basis function). In case a full-band DPD is used to linearize the two aggregated CCs, the DPD memory order $N = 3$ (i.e., four taps per basis function).

B. Base Station Measurements

Three different LTE-A RF measurement scenarios are presented in this section. The first, is a contiguous intraband CA scenario, the second is a noncontiguous intraband CA scenario, while the third is an interband CA scenario. In the first two scenarios, a commercial LTE-A Band 1 (2110-2170 MHz) BS PA is used, shown in Fig. 5(c). The freescale BS PA (model no. MD7IC2250GN) is a Doherty PA with 31 dB gain, and +47 dBm 1 dB compression point. A driver amplifier is used before the Doherty PA with 14 dB gain and +25 dBm 1 dB compression point. In the third scenario, a general-purpose wideband PA with 40 dB gain, and +28 dBm 1 dB compression point is used, as shown in Fig. 5(d). This PA (model no. ZHL-

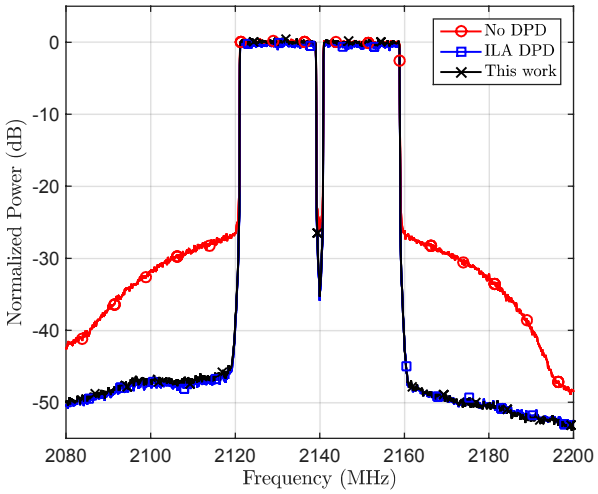

Fig. 6. An RF measurement example at LTE DL Band 1 (2110-2170 MHz) showing the normalized PA output spectra of a contiguous intraband CA transmitter with two 20 MHz OFDM carriers. 16-QAM subcarrier modulation is used per CC. Spectral regrowth and EVM are reduced when using the proposed decorrelation-based DPD with a real commercial base station PA operating at +36 dBm output power.

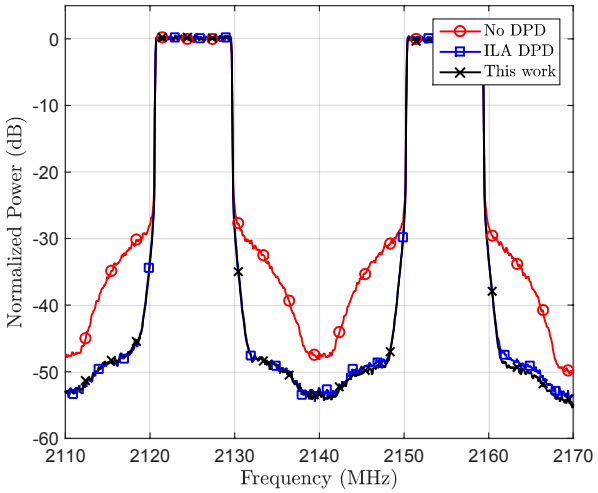

Fig. 8. An RF measurement example at LTE DL Band 1 (2110-2170 MHz) showing the normalized PA output spectra of a concurrent noncontiguous intraband CA transmitter with two 10 MHz OFDM carriers. The CC spacing is 30 MHz, and 16-QAM subcarrier modulation is used. Spectral regrowth and EVM are reduced when using the proposed decorrelation-based concurrent DPD with a real commercial base station PA operating at +34 dBm TX power.

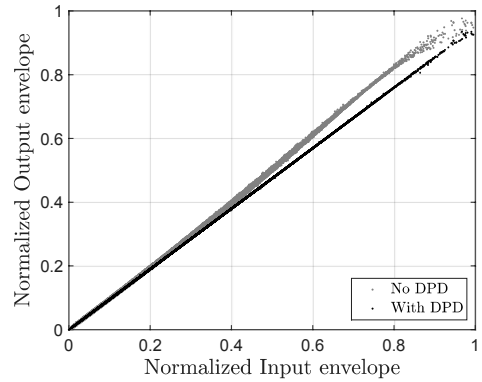

(a) AM AM response

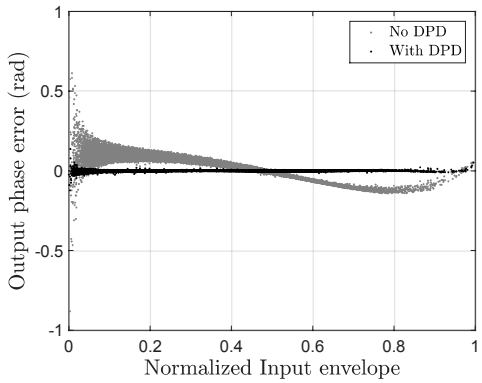

(b) AM PM response

Fig. 7. AM/AM and AM/PM responses of the LTE-A DL Doherty BS PA with (black) and without (gray) the proposed DPD at +36 dBm output power.

4240) is suitable for interband CA, and can, in principle, be adopted, e.g., in femto-cell access points.

1) Contiguous Intraband CA Scenario: An LTE-A Band 1 contiguous intraband CA scenario with two 20 MHz CCs is studied, in which the two aggregated CCs are interpreted as one CC (i.e, CC1), as explained in Section IV-B. The aggregated signal is transmitted via one RF transmitter (TX) chain of the AD evaluation board, and thus no RF combiner is used in this scenario. The block-adaptive DPD processing is implemented on a host processor, using the full-band baseband I/Q samples from the observation receiver, with 200 MHz observation BW. Iterative clipping and filtering -based PAPR reduction is applied to the composite transmit signal in this scenario [33]. The classical ILA-based DPD is also implemented for reference, and compared to the proposed DPD in Fig. 6, with Table IV showing the corresponding ACLR and EVM results. As is obvious, the proposed DPD solution and the existing ILA-based DPD are both providing very similar performance, despite the substantial difference in the computing complexity in favor of the proposed solution, as already demonstrated in Section V. Fig. 7 shows the AM/AM and AM/PM responses of the PA with the proposed DPD (black), and without DPD (gray), in this scenario, measured at +36 dBm average output power.

2) Noncontiguous Intraband CA Scenario: An LTE-A Band 1 noncontiguous intraband CA scenario, with two 10 MHz CCs and 30 MHz carrier spacing, is studied next. Each CC is transmitted via a separate RF chain in this scenario, and an RF combiner is then used to combine the two CCs at the PA input, as also illustrated in Fig. 5. 30 MHz observation BW is used per CC in the proposed DPD learning, which is done sequentially, one CC at a time in this example, unlike in the previous contiguous scenario where the whole aggregated signal was used for learning. The final DPD coefficients after convergence are then applied on each CC before being

TABLE IV
BS RF MEASUREMENT SCENARIOS AND OBTAINED RESULTS

Scenario	DPD Type	EVM [%]	ACLR L / R of CC1 (dBc)	ACLR L / R of CC2 (dBc)	TX Power (dBm)	PAPR (dB)
Contiguous Intraband CA	No DPD	5.65	30.89 / 31.56	N/A	+36	8.8
	ILA DPD	1.97	46.87 / 49.66	N/A	+36	8.8
	This work	2.04	46.95 / 50.12	N/A	+36	8.8
Noncontiguous Intraband CA	No DPD	5.54	36.60 / 36.63	36.41 / 36.36	+34	9.87
	ILA DPD	1.85	49.85 / 48.72	49.99 / 49.85	+34	9.87
	This work	1.93	49.89 / 49.33	49.98 / 49.87	+34	9.87
Noncontiguous Interband CA	No DPD	3.92	35.47 / 36.08	36.36 / 35.95	+23	9.94
	[10]	1.24	48.05 / 48.10	48.16 / 48.12	+22	9.94
	[14], [15]	1.25	48.05 / 48.09	48.15 / 48.12	+22	9.94
	This work	1.28	50.07 / 49.95	49.13 / 49.08	+23	9.94

transmitted via the corresponding TX chains. Iterative clipping and filtering -based PAPR reduction is applied to each CC separately in this scenario. The classical full-band ILA-based DPD is also implemented for reference, with block LS based parameter learning per ILA iteration, and compared to the proposed concurrent DPD in Fig. 8, with Table IV showing the corresponding ACLR and EVM results. The linearization performance numbers are again very similar despite the proposed concurrent DPD being significantly less complex than the full-band ILA-based DPD, as analyzed already in Section V.

3) Interband CA Scenario: For further demonstration and proof-of-concept of the proposed concurrent DPD, a true interband CA scenario is addressed next. The setup is otherwise similar to the previous setup related to the noncontiguous intraband CA scenario, but, in this case, the two aggregated CCs are located at Band 2 (1930-1990 MHz), and Band 4 (2110-2155 MHz), respectively, which is a practical LTE-A interband CA scenario [34]. Furthermore, the general purpose wideband PA is used. Iterative clipping and filtering -based PAPR reduction is again applied to each CC separately. The performance of the proposed single feedback concurrent DPD is compared against two different concurrent DPD techniques: the first is the classical concurrent DPD reported in [10] with two feedback receivers, and the second is the single feedback concurrent DPD developed in [14], [15].

Fig. 9 shows the normalized spectra at the PA output without DPD and with the three considered concurrent DPD techniques, at +23 dBm PA output power. An extra 1 dB backoff is applied in the concurrent DPDs in [10], [14], [15] for proper operation, however, such backoff is not required for the proposed DPD which does not use the ILA principle for learning. The results in Fig. 9 and Table IV again demonstrate very good linearization performance of the proposed concurrent DPD solution, which is even slightly better than the other concurrent DPDs, despite its reduced complexity, as explained in Section V. The same assumptions that were made in Section V are assumed here as well for a fair comparison among the considered concurrent DPD techniques.

C. UE Measurements

Two different LTE-A UE RF measurement scenarios are presented in this section. The first corresponds to 3GPP LTE-A multicluster transmission scenario [4], while the second is a noncontiguous intraband CA scenario where only one of the CCs and one of the IM3 spurs are being linearized, thus demonstrating the flexibility of the proposed DPD. The power amplifier adopted in the UE RF measurements (model no. ACPM-5002-TR1) is designed for LTE-A UL Band 25 (1850-1915 MHz), with 29 dB gain, and +31 dBm 1 dB compression point, as shown in Fig. 5(e).

1) Multicluster Scenario: Fig. 10 demonstrates an RF measurement example corresponding to 3GPP LTE-Advanced multicluster transmission scenario, where the mobile device is accessing a single SC-FDMA based 20 MHz LTE UL carrier with non-contiguous physical resource block (PRB) allocation inside the carrier. The figure shows the normalized spectra at the PA output, with and without the proposed DPD, operating at +24 dBm TX power. A single full-band decorrelation-based DPD is used, in this scenario, to linearize the overall signal composed of the two clusters, with 5 MHz and 10 MHz bandwidths and 5 MHz cluster separation. Iterative clipping and filtering based PAPR reduction is applied to the composite transmit signal. ILA based DPD is also implemented and compared to the proposed DPD in Table V, in terms of the ACLR and EVM, demonstrating similar performance between them.

2) Noncontiguous Intraband CA Scenario: Fig. 11 represents a scenario where also the negative IM3 sub-band is emitted inband (not suppressed by the TX/antenna filter), while the positive IM3 sub-band is out-of-band and can thus be easily filtered by the TX filter. The two SC-FDMA based UL component carriers in this example have 10 MHz and 5 MHz bandwidths, where the 10 MHz CC uses QPSK data modulation, while the 5 MHz CC uses 64QAM data modulation, and is thus much more sensitive to EVM degradation. In this example, the DPD is therefore deliberately configured to linearize only the 5 MHz component carrier and the negative IM3 sub-band, which is emitted inband, to demonstrate the great processing and linearization flexibility. 25 MHz observation BW is used in the proposed DPD learning, such that the DPD coefficients to linearize CC2 and the negative IM3 sub-band are learned sequentially. Iterative clipping and filtering based PAPR reduction is applied to the ideal transmit signal. Table V shows the ACLR, EVM and IM3 spur suppression results in this scenario, evidencing again very high-performance linearization. Notice that the IM spur at the negative IM3 sub-band is also suppressed by around 20 dB through the DPD

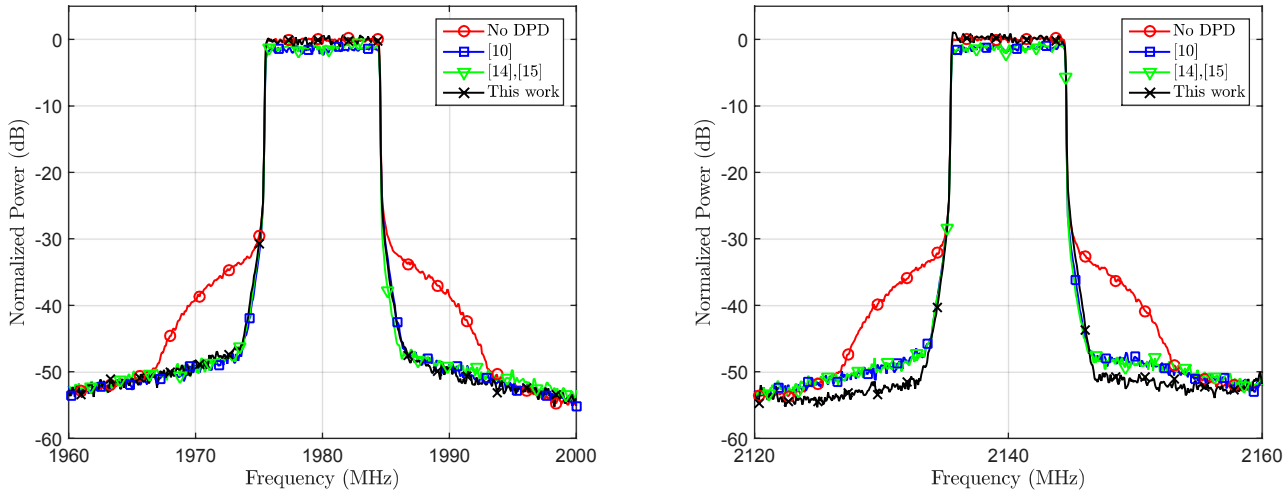

(a) (b)

Fig. 9. A practical LTE-A DL interband CA RF measurement example showing the normalized PA output spectra with and without DPD using a real commercial wideband PA operating at +23 dBm output power. The OFDM CCs are 10 MHz each and transmitted at LTE-A DL bands 2 (1930-1990 MHz) and 4 (2110-2155 MHz) respectively, with 160 MHz CC spacing. 16-QAM subcarrier modulation is used per CC. Spectral regrowth and EVM are reduced when using the proposed decorrelation-based concurrent DPD, which slightly outperforms the concurrent DPDs in [10], [14], [15].

TABLE V
UE RF MEASUREMENT SCENARIOS AND OBTAINED RESULTS

TX Power = +24 dBm **Scenario**	DPD Type	EVM [%]	ACLR L / R of CC1 (dBc)	ACLR L / R of CC2 (dBc)	IM3- spur supression (dB)	PAPR (dB)
Multicluster	No DPD	4.39	32.04 / 34.23	N/A	N/A	8.65
	ILA DPD	0.71	45.98 / 47.31	N/A	N/A	8.65
	This work	0.79	46.28 / 47.28	N/A	N/A	8.65
Noncontiguous Intraband CA	No DPD	3.68	N/A	33.43 / 33.95	0	8.18
	This work	0.73	N/A	50.26 / 50.47	20	8.18

processing, taking it below the general spurious emission limit of -30 dBm/1MHz measurement bandwidth that all RF devices must obey [35].

D. Discussion and Future Work

In this section, we shortly point towards some future work items in the context of the proposed concurrent DPD solution. Despite the fact that the proposed solution is already offering excellent linearization performance at substantially reduced complexity compared to other state-of-the-art concurrent DPD methods, as demonstrated through extensive simulations and RF measurements, there is potentially some room for further improvements.

The fact that the learning of the DPD coefficients for the two CCs is done sequentially can, in principle, cause some inter-dependence between the optimal coefficients of the DPD stages of CC1 and CC2, in particular if the PA is very deep in saturation. Specifically, in very deep saturation, and assuming that the DPD coefficients of CC1 are learned first, then activating the DPD unit of CC2 may cause slight degradation of the linearization of CC1. We hypothesize that then iterating shortly the learning between the CCs can reduce this mutual effect while reaching an improved linearization performance for the CCs. On the other hand, this may require somewhat more learning samples in the overall learning procedure. In the context of the described learning rules, these iterations between the CCs can basically be adopted at the level of the learning block m or then between the K learning blocks of individual CCs, assuming that the observation receiver center-frequency can be adjusted accordingly.

We also wish to acknowledge that it is basically also possible to perform the learning for the two CCs in parallel, instead of sequentially, while still using only a single narrowband observation receiver. However, this will require storing the PA observation samples and basis function samples of one of the two CCs in memory in order to allow learning the DPD coefficients for CC1 and CC2 simultaneously. With such parallel learning, however, the actual parameter learning algorithms are to be re-designed. This is one interesting topic for our future work.

Another interesting point for future work is extending the proposed concurrent DPD to support transmitting more than two component carriers. The decorrelation-based learning, as such, can support any number of bands or CCs, but the basis functions for scenarios with more than two CCs will be different. In this context, it is worth mentioning that a concurrent DPD solution for tri-band CA scenarios has been developed in [36]. The mathematical expressions representing

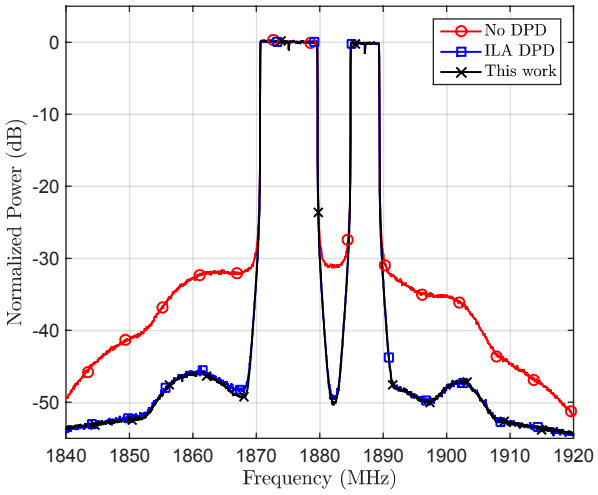

Fig. 10. An RF measurement example at LTE UL band 25 (1850-1915 MHz) showing the normalized spectra of a multicluster 20 MHz SC-FDMA signal with 16-QAM data modulation at 1880 MHz. Spectral regrowth and EVM are reduced when using the proposed decorrelation-based DPD with a real commercial mobile PA operating at +24 dBm output power. ILA based DPD is also implemented and shown for reference.

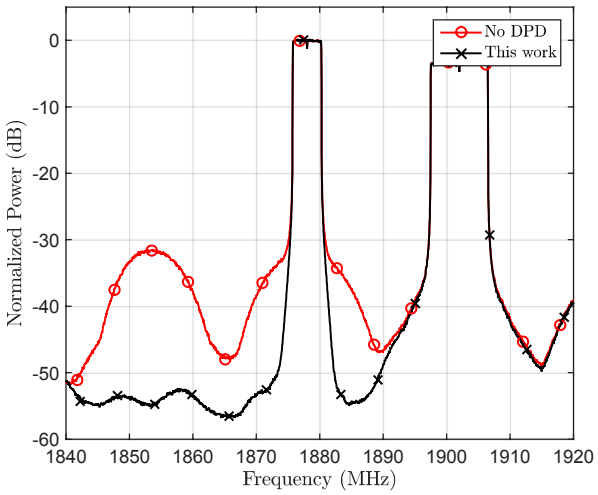

Fig. 11. An RF measurement example at LTE UL band 25 (1850-1915 MHz) showing the normalized PA output spectra of a concurrent noncontiguous intraband CA transmitter with 10 MHz and 5 MHz SC-FDMA component carriers, using QPSK and 64-QAM data modulation respectively. Nonlinear distortion at and around the 5 MHz CC as well as at the IM3- sub-band are reduced when using the proposed decorrelation-based DPD with a real commercial mobile PA operating at +24 dBm output power.

the nonlinear distortion components are derived in [36] from a pruned Volterra model, while the DPD learning is based on the classical indirect learning architecture. Finally, extending the developed concurrent DPD structure and parameter learning principles to account also for I/Q modulators' impairments, e.g., through augmented sets of basis functions, like was done in [37] in more ordinary single-band transmitter context, is one interesting and important future study topic.

VIII. Conclusions

In this article, a novel decorrelation-based concurrent digital predistortion (DPD) solution was proposed for suppressing nonlinear distortion in dual carrier transmitters where a single power amplifier (PA) is used to amplify both carriers. The proposed solution adopts only a single narrowband feedback path, opposed to many earlier concurrent DPD solutions which commonly require a separate feedback path per carrier, such that closed-loop decorrelation based parameter learning is carried out in a per carrier or per band manner. The decorrelation-based closed-loop learning and linearization were also shown to be fully applicable in more classical single carrier or single band transmitters. Furthermore, a flexible overall linearization architecture was introduced where the concurrent linearization at and around the main carriers was complemented with additional predistortion branches to suppress spurious emissions more far away from the main carriers. The combined solution offers great flexibility in mitigating and suppressing nonlinear distortion at any desired sub-band(s), while still using a single feedback receiver. The linearization performance was evaluated in a comprehensive manner using both simulations and actual RF measurements, incorporating both UE side and BS side LTE/LTE-Advanced power amplifiers and different contiguous and non-contiguous transmission scenarios. All experiments demonstrated excellent linearization performance, despite the very simple processing and substantially lower hardware and computing complexities compared to existing solutions.

References

[1] C. Park, L. Sundström, A. Wallen, and A. Khayrallah, "Carrier aggregation for LTE-advanced: Design challenges of terminals," *IEEE Commun. Mag.*, pp. 76–84, Dec. 2013.

[2] S.A. Bassam, W. Chen, M. Helaoui, and F.M. Ghannouchi, "Transmitter architecture for CA: Carrier Aggregation in LTE-Advanced systems," *IEEE Microw. Mag.*, vol. 14, 2013.

[3] P. Roblin, C. Quindroit, N. Naraharisetti, S. Gheitanchi, and M. Fitton, "Concurrent linearization," *IEEE Microw. Mag.*, pp. 75–91, Nov. 2013.

[4] *LTE Evolved Universal Terrestrial Radio Access (E-UTRA) User Equipment (UE) radio transmission and reception, 3GPP TS 36.101 V12.4.0 (Release 12)*, June 2014.

[5] Nokia, "R4-121205 Way forward for non-contiguous intraband transmitter aspects. Available at: http://www.3gpp.org/," Tech. Rep., 3GPP, Feb. 2013.

[6] Nokia, "R4-124353, Non-contiguous intraband unwanted emission. Available at: http://www.3gpp.org/," Tech. Rep., 3GPP, Feb. 2013.

[7] Ericsson and ST-Ericsson, "R4-123797, UE reference sensitivity requirements with two UL carriers. Available at: http://www.3gpp.org/," Tech. Rep., 3GPP, Feb. 2013.

[8] C. Yu, W. Cao, Y. Guo, and A. Zhu, "Digital Compensation for Transmitter Leakage in Non-Contiguous Carrier Aggregation Applications With FPGA Implementation," *IEEE Trans. Microw. Theory Techn.*, vol. 63, no. 12, pp. 4306–4318, Dec 2015.

[9] A. Kiayani, M. Abdelaziz, L. Anttila, V. Lehtinen, and M. Valkama, "Digital Mitigation of Transmitter-Induced Receiver Desensitization in Carrier Aggregation FDD Transceivers," *IEEE Trans. Microw. Theory Techn.*, vol. 63, no. 11, pp. 3608–3623, Nov 2015.

[10] S.A. Bassam, F.M. Ghannouchi, and M. Helaoui, "2-D Digital Predistortion (2-D-DPD) architecture for concurrent dual-band transmitters," *IEEE Trans. Microw. Theory Techn.*, vol. 59, pp. 2547–2553, Oct. 2011.

[11] Y. J. Liu, W. Chen, J. Zhou, B. H. Zhou, and F. M. Ghannouchi, "Digital Predistortion for Concurrent Dual-Band Transmitters Using 2-D Modified Memory Polynomials," *IEEE Trans. Microw. Theory Techn.*, vol. 61, no. 1, pp. 281–290, Jan 2013.

[12] Hua Qian, Saijie Yao, Hao Huang, Xiumei Yang, and Weifeng Feng, "Low complexity coefficient estimation for concurrent dual-band digital predistortion," *IEEE Trans. Microw. Theory Techn.*, vol. 63, no. 10, pp. 3153–3163, Oct 2015.

[13] M. Cabarkapa, N. Neskovic, and D. Budimir, "A Generalized 2-D Linearity Enhancement Architecture for Concurrent Dual-Band Wireless Transmitters," *IEEE Trans. Microw. Theory Techn.*, vol. 61, no. 12, pp. 4579–4590, Dec 2013.

[14] Y. Liu, J. Yan, and P. Asbeck, "Concurrent dual-band digital predistortion with a single feedback loop," *IEEE Trans. Microw. Theory Techn.*, vol. 63, no. 5, pp. 1556–1568, May 2015.

[15] Yuelin Ma and Y. Yamao, "Spectra-Folding Feedback Architecture for Concurrent Dual-Band Power Amplifier Predistortion," *IEEE Trans. Microw. Theory Techn.*, vol. 63, no. 10, pp. 3164–3174, Oct 2015.

[16] C. Yu, J. Xia, X. Zhu, and A. Zhu, "Single-Model Single-Feedback Digital Predistortion for Concurrent Multi-Band Wireless Transmitters," *IEEE Trans. Microw. Theory Techn.*, vol. 63, no. 7, pp. 2211–2224, July 2015.

[17] M. Abdelaziz, L. Anttila, A. Mohammadi, F. Ghannouchi, and M. Valkama, "Reduced-complexity power amplifier linearization for carrier aggregation mobile transceivers," in *IEEE International Conference on Acoustics, Speech, and Signal Processing*, May 2014.

[18] M. Abdelaziz, L. Anttila, C. Tarver, K. Li, J. Cavallaro, and M. Valkama, "Low-Complexity Sub-band Digital Predistortion for Spurious Emission Suppression in Noncontiguous Spectrum Access," *IEEE Trans. Microw. Theory Techn.*, vol. 64, no. 11, pp. 3501–3517, Nov. 2016.

[19] C. Yu, M. Allegue-Martnez, Y. Guo, and A. Zhu, "Output-Controllable Partial Inverse Digital Predistortion for RF Power Amplifiers," *IEEE Trans. Microw. Theory Techn.*, vol. 62, no. 11, pp. 2499–2510, Nov 2014.

[20] Z. Fu, L. Anttila, M. Abdelaziz, M. Valkama, and A. Wyglinski, "Frequency-selective digital predistortion for unwanted emission reduction," *IEEE Trans. Commun.*, vol. 63, no. 1, pp. 254–267, Jan. 2015.

[21] A.S. Tehrani, H. Cao, S. Afsardoost, T. Eriksson, M. Isaksson, and C. Fager, "A comparative analysis of the complexity/accuracy tradeoff in power amplifier behavioral models," *IEEE Trans. Microw. Theory Techn.*, vol. 58, pp. 1510–1520, June 2010.

[22] J. Liu, J. Zhou, W. Chen, B. Zhou, and F.M. Ghannouchi, "Low-complexity 2D behavioural model for concurrent dual-band power amplifiers," *Electronics Letters*, vol. 48, no. 11, pp. 620–621, May 2012.

[23] H. Q. He and M. Faulkner, "Performance of adaptive predistortion with temperature in RF power amplifier linearization," in *Proceedings of the Fifth International Symposium on Signal Processing and Its Applications.*, 1999, vol. 2, pp. 717–720.

[24] S. Haykin, *Adaptive Filter Theory, Fifth Edition*, Pearson, 2014.

[25] W. Hoffmann, "Iterative algorithms for Gram Schmidt orthogonalization," *Computing*, vol. 41, no. 4, pp. 335–348, 1989.

[26] M. Abdelaziz, C. Tarver, K. Li, L. Anttila, M. Valkama, and J. Cavallaro, "Sub-band digital predistortion for noncontiguous transmissions: Algorithm development and real-time prototype implementation," in *49th Asilomar Conf. Signals, Systems, and Computers, Pacific, Grove, CA, USA.*, Nov. 2015.

[27] E. Zenteno and D. Rönnow, "MIMO Subband Volterra Digital Predistortion for Concurrent Aggregated Carrier Communications," *IEEE Trans. Microw. Theory Techn.*, vol. 65, no. 3, pp. 967–979, March 2017.

[28] C. Yu, L. Guan, E. Zhu, and A. Zhu, "Band-Limited Volterra Series-Based Digital Predistortion for Wideband RF Power Amplifiers," *IEEE Trans. Microw. Theory Techn.*, vol. 60, no. 12, pp. 4198–4208, Dec 2012.

[29] R. Raich, Hua Qian, and G. T. Zhou, "Orthogonal polynomials for power amplifier modeling and predistorter design," *IEEE Trans. Veh. Technol.*, vol. 53, no. 5, pp. 1468–1479, Sept 2004.

[30] R. Raich and G. T. Zhou, "Orthogonal polynomials for complex gaussian processes," *IEEE Trans. Signal Process.*, vol. 52, no. 10, pp. 2788–2797, Oct 2004.

[31] Alan V. Oppenheim and Ronald W. Schafer, *Discrete-Time Signal Processing, 3rd Edition*, Prentice Hall, 1999.

[32] E. Dahlman, S. Parkvall, and J. Skold, *4G LTE/LTE-Advanced for Mobile Broadband.*, Elsevier Ltd., 2011.

[33] J. Armstrong, "Peak-to-average power reduction for OFDM by repeated clipping and frequency domain filtering," *Electronics Letters*, vol. 38, no. 5, pp. 246–247, Feb 2002.

[34] *LTE Evolved Universal Terrestrial Radio Access (E-UTRA) Base Station (BS) radio transmission and reception, 3GPP TS 36.104 V12.6.0 (Release 12)*, Feb 2015.

[35] *International Telecommunication Union Radio Communication Sector, Recommendation ITU-R SM.329-12 Unwanted emissions in the spurious domain. Available at: https://www.itu.int/.*

[36] M. Younes, A. Kwan, M. Rawat, and F. M. Ghannouchi, "Linearization of Concurrent Tri-Band Transmitters Using 3-D Phase-Aligned Pruned Volterra Model," *IEEE Trans. Microw. Theory Techn.*, vol. 61, no. 12, pp. 4569–4578, Dec 2013.

[37] L. Anttila, P. Händel, and M. Valkama, "Joint mitigation of power amplifier and I/Q modulator impairments in broadband direct-conversion transmitters," *IEEE Trans. Microw. Theory Techn.*, vol. 58, pp. 730–739, April 2010.

Mahmoud Abdelaziz (S'13) received his B.Sc. (hons.) and M.Sc. degrees in Electronics and Communications Engineering from Cairo University, Egypt, in 2006 and 2011, respectively. He is currently pursuing the D.Sc. degree at Tampere University of Technology, Finland where he works as a researcher with the Department of Electronics and Communications. From 2007 to 2012 he has worked at California-based Newport Media Inc., as well as other companies in the wireless industry. His research interests include statistical and adaptive signal processing in flexible radio transceivers, and wideband digital predistortion.

Lauri Anttila (S'06, M'11) received the M.Sc. degree and D.Sc. (Tech) degree (with honors) in electrical engineering from Tampere University of Technology (TUT), Tampere, Finland, in 2004 and 2011. Currently, he is a Senior Research Fellow at the Department of Electronics and Communications Engineering at TUT. His research interests are in signal processing for wireless communications, in particular radio implementation challenges in 5G cellular radio and full-duplex radio, flexible duplexing techniques, and transmitter and receiver linearization. He has co-authored over 60 peer reviewed articles in these areas, as well as two book chapters.

Adnan Kiayani received the B.Sc. degree from COMSATS Institute of Information Technology, Islamabad, Pakistan, in 2006, the M.Sc. degree (with honors) and D.Sc. degree from Tampere University of Technology (TUT), Tampere, Finland, in 2009 and 2015, respectively, all in electrical engineering. He is currently a post-doctoral research fellow at the Department of Electronics and Communications Engineering, TUT, working on the self-interference cancellation in frequency division duplex (FDD) transceivers using digital signal processing (DSP) techniques. His general research interests are in analysis and DSP algorithms for wireless communications, including RF impairments mitigation.

Mikko Valkama (S'00, M'01, SM'15) was born in Pirkkala, Finland, on November 27, 1975. He received the M.Sc. and Ph.D. Degrees (both with honors) in electrical engineering (EE) from Tampere University of Technology (TUT), Finland, in 2000 and 2001, respectively. In 2003, he was working as a visiting researcher with the Communications Systems and Signal Processing Institute at SDSU, San Diego, CA. Currently, he is a Full Professor and Department Vice-Head at the Department of Electronics and Communications Engineering at TUT, Finland. His general research interests include radio communications, radio networks and communications signal processing, with specific emphasis on 5G mobile communications systems.